WILEY-VCH

DOI: 10.1002/ ((please add manuscript number))
Article type: Full Article

Voltage-induced coercivity reduction in nanoporous alloy films: a boost towards energy-efficient magnetic actuation

Alberto Quintana, Jin Zhang, Eloy Isarain-Chávez, Enric Menéndez, Ramon Cuadrado, Roberto Robles, Maria Dolors Baró, Miguel Guerrero, Salvador Pané, Bradley James Nelson, Carlos Maria Müller, Pablo Ordejón, Josep Nogués*, Eva Pellicer*, Jordi Sort**

A. Quintana, Dr. J. Zhang, Dr. E. Isarain-Chávez, Dr. E. Menéndez, Prof. M. D. Baró, Dr. M. Guerrero, Dr. E. Pellicer
Departament de Física, Universitat Autònoma de Barcelona, E-08193 Cerdanyola del Vallès, Spain
E-mail: Eva.Pellicer@uab.cat
R. Cuadrado, Dr. R. Robles, Prof. P. Ordejón
Catalan Institute of Nanoscience and Nanotechnology (ICN2), CSIC and The Barcelona Institute of Science and Technology, Campus UAB, Bellaterra, E-08193 Barcelona, Spain
E-mail: Roberto.Robles@icn2.cat
Dr. S. Pané, Prof. B. J. Nelson
Institute of Robotics and Intelligent Systems (IRIS), ETH Zürich, CH-8092 Zürich, Switzerland
Prof. C.M. Müller
Departament de Ciència de Materials i Química Física, Universitat de Barcelona, Martí i Franquès 1, E-08028, Barcelona, Catalonia, Spain
Prof. J. Nogués
Catalan Institute of Nanoscience and Nanotechnology (ICN2), CSIC and The Barcelona Institute of Science and Technology, Campus UAB, Bellaterra, E-08193 Barcelona, Spain
ICREA, Pg. Lluís Companys 23, E-08010 Barcelona, Spain
E-mail: Josep.Nogues@icn2.cat
Prof. J. Sort
Departament de Física, Universitat Autònoma de Barcelona, E-08193 Cerdanyola del Vallès, Spain
ICREA, Pg. Lluís Companys 23, E-08010 Barcelona, Spain
E-mail: Jordi.Sort@uab.cat

Keywords: nanoporous alloys, magnetic actuation, magneto-electric effect, coercivity, energy efficiency

Abstract

Magnetic data storage and magnetically actuated devices are conventionally controlled by magnetic fields generated using electric currents. This involves significant power dissipation by Joule heating effect. To optimize energy efficiency, manipulation of magnetic information with lower magnetic fields (i.e., lower electric currents) is desirable. This can be accomplished by reducing the coercivity of the actuated material. Here, a drastic reduction of coercivity is observed at room temperature in thick (~600 nm), nanoporous, electrodeposited Cu-Ni films by simply subjecting them to the action of an electric field. The effect is due to voltage-induced changes in the magnetic anisotropy. The large surface-area-to-volume ratio and the ultra-narrow pore walls of the system allow the whole film, and not only the topmost surface, to effectively contribute to the observed magnetoelectric effect. This waives the stringent ´ultrathin-film requirement´ from previous studies, where small voltage-driven coercivity variations were reported. This observation expands the already wide range of applications of nanoporous materials (hitherto in areas like energy storage or catalysis) and it opens new paradigms in the fields of spintronics, computation and magnetic actuation in general.

1. Introduction

The continuous progress in information and communication technologies critically depends on an optimized utilization of electric power. Magnetism and spintronics have largely contributed to the digital revolution by dramatically enhancing the hard disk capacity and the data processing speed.[1,2] Magnetic actuation is also at the heart of many micro/nano-electromechanical systems and other engineering applications. However, power consumption in magneto-electronic devices continues to be a constraining issue.[3] Magnetization switching in devices is conventionally done by localized magnetic fields (generated via electromagnetic induction) or by spin-polarized electric currents (spin-transfer torque).[2,4] Both principles

require of relatively high electric currents and therefore involve significant loss of energy in the form of heat dissipation (Joule effect). For example, the currents needed to operate conventional magnetic random-access memories (MRAMs) are of the order of 10 mA, whereas spin-transfer torque MRAMs require currents of at least 0.5 mA. This is still a factor five times larger than the output currents delivered by highly miniaturized metal-oxide-semiconductor field-effect transistors.[5] Replacement of electric currents by electric fields would drastically contribute to reduce the overall power consumption in these and other devices.

Several approaches to tailor magnetism by means of an electric field have been proposed so far: (i) strain-mediated magnetoelectric coupling in piezoelectric-magnetostrictive composite materials,[6,7] (ii) multiferroic materials in which the ferroelectric and ferromagnetic order parameters are coupled to each other[8] and (iii) electric-field induced oxidation-reduction transitions (magneto-ionics).[9,10] However, each of these approaches faces some drawbacks, e.g., (i) clamping effects with the substrate, need of epitaxial interfaces and risk of fatigue-induced mechanical failure, (ii) the dearth of available multiferroic materials and the reduced strength of magnetoelectric coupling, even at low temperatures and (iii) precise control of the chemical reactions, their kinetics, and the reversibility of the process. Thus, there is clearly a technological demand for alternative approaches to manipulate magnetism with an electric field at room temperature.

Interestingly, a number of exciting experiments performed in recent years have shown the possibility to modify the magnetic properties of diluted magnetic semiconductors[11,12] and some metallic elements and alloys[13-16] directly with an applied electric field, via accumulation of electrostatic charges at their surface. This is very promising for the development of low-power magnetic actuators and spintronic devices. Among the magnetic effects caused by electric field one can mention: change of Curie temperature in diluted

magnetic semiconductors such as (Ga,Mn)As or (In,Mn)As[11]; changes of coercivity[11,17] and, in some cases, reorientation of the magnetic easy axis in thin films.[12,18] In semiconductors these effects are mostly observed at low temperatures and are due to electric-field induced modification of the charge carriers' concentration. In metals, magnetoelectric phenomena are related to spin-dependent screening (i.e., electrons with different spin characters respond differently to the applied electric field[16]) and, therefore, only occur within a few nm from the surface[19]. This restricts the effect to ultra-thin films (consisting of a few monolayers)[13-15,17,18], difficult to be integrated in real devices.

Given the surface origin of voltage-induced magnetic changes in metals, it is envisaged that an increase of the surface area-to-volume ratio in nanoporous materials could trigger a significant enhancement of magnetoelectric effects, provided that the pore walls are kept sufficiently narrow[20,21]. During the last few years, the advances in the synthetic pathways to produce nanoporous materials with controllable pore size and composition have boosted a wealth of applications in diverse fields such as catalysis, bioimplants, dampers, gas sensing or energy storage, where materials with a high surface area are essential.[22-24] However, although many of the cutting-edge technological applications in spintronics and magnetic actuators also rely on surface or interface magnetic phenomena, the use of nanoporous materials in these technologically-relevant fields has been largely overlooked,[25,26] particularly for pure magnetoelectric effects, i.e., neither mediated by strain nor resulting from oxidation/reduction reactions.

In this work, we explore intrinsic magnetoelectric effects in nanoporous Cu-Ni films grown by micelle-assisted electrodeposition (**Figure 1a**). We demonstrate that a drastic reduction of coercivity can be obtained in the nanoporous metallic alloy (with very narrow pore walls) under the application of voltage across an electrical double layer using a non-aqueous liquid electrolyte. The nanoporous morphology of the investigated material allows for much larger accumulation of surface electric charges compared to fully-dense films. Since

the whole porous structure is affected by the electric field, this results in a much more pronounced voltage-induced reduction of coercivity compared to previous studies.[13] The purely magnetoelectric effects in Cu-Ni are ascribed by *ab-initio* calculations to changes in the magnetic anisotropy energy stemming from electric field-induced spin-dependent modifications of the magnetic density of states at the surface.

2. Results and Discussion

2.1. Morphology and structure of the electrodeposited films

The typical morphology of the cross-section of the electrodeposited Cu-Ni films, observed by scanning transmission electron microscopy (STEM), is shown in Figure 1b. STEM observations demonstrate the occurrence of open-cell porosity, with highly interconnected ligaments whose lateral size is typically around 5-7 nm. The overall film's thickness is around 600 nm. Further structural analysis, performed by high-resolution transmission electron microscopy (HRTEM), reveals the occurrence of crystalline planes within the pore walls (Figure 1c). The corresponding selected area electron diffraction (SAED) patterns (Figure 1d) indicate the formation of a face-centered cubic (FCC) solid solution, similar to electrodeposited Cu-Ni.[27] X-ray diffraction (XRD) measurements (Figure 1e) corroborate that the films grow forming a FCC solid solution and they are actually textured along the (111) direction, i.e., the (200) FCC peak, expected at around 2θ = 51-52º, is not detected.[27] Moreover, even if the free energy of mixing between Cu and Ni is slightly positive[28], no phase separation into Cu-rich and Ni-rich regions takes place during electrodeposition. Compositional analyses, carried out by energy-dispersive X-ray (EDX) spectroscopy, reveal that the composition of the films is $Cu_{25}Ni_{75}$ (at. %). The nanoporous character of the Cu-Ni films brings about a drastic increase of the surface area-to-volume ratio (S/V). Indeed, simple geometrical reasoning can be used to show, for example, that the S/V ratio of a 600 nm–thick porous film covering an area of 1 × 1 mm^2 and being made of an

array of vertically-oriented pores, with 5 nm pore diameter and 5 nm interpore distance would be about 120 times larger than the S/V ratio of a fully-dense layer of 600 nm covering the same area. Interestingly, the total volume of "active material" (i.e., influenced by the action of an electric field) in the nanoporous layer case would be around 250 times larger than that of an ultra-thin (2 nm thick) film.

2.2. Control of coercivity using voltage

Figure 2a illustrates the experimental setup used for the magnetoelectric measurements. The formation of the electrical double layer surrounding the pore walls is depicted in Figure 2b. The sample was mounted in a home-made electrolytic cell filled with anhydrous propylene carbonate with Na^+ solvated species, and the magnetic properties were measured along the film plane by magneto-optic Kerr effect (MOKE), while applying different constant voltages between the sample and the counter-electrode. The use of a liquid electrolyte is very convenient to generate high electric fields. Namely, the large dielectric constant (ε_r = 64 for propylene carbonate) and the formation of the so-called electrical double-layer (with thickness ~1 nm)[29] promote significant charging effects when applying moderate voltages. Representative hysteresis loops, measured at different positive voltages, from 0 V to 14 V, are shown in Figure 2c. A progressive narrowing of the hysteresis loop is clearly observed as the voltage is increased. The coercivity, H_C, decreases from approximately 97 Oe to 66 Oe, which represents a relative variation close to 32% (see **Figure 3a**). This is a remarkably larger change compared to previous works from the literature on ultra-thin metallic films, reporting variations of only up to 4.5%.[13] The loops also tend to become progressively more square-shaped as the applied voltage is increased. The corresponding variation of the remanence-to-saturation magnetization ratio, M_R/M_S, and the normalized differential magnetic susceptibility around the coercivity, $\chi = (dm/dH)_{H=HC}$ (where m denotes here the normalized Kerr amplitude signal) are shown in Figure 3b. The effects on H_C, M_R/M_S

and χ for negative voltages are significantly smaller and opposite to those observed with positive voltage (see Figure S1 in the Supporting Information). No significant variations in the Kerr signal amplitude were observed for either positive or negative applied voltages. To corroborate the crucial role played by the porosity on the observed magnetoelectric effects, the same experiments were performed on fully-dense Cu-Ni films with the same composition and thickness, prepared by electrodeposition. As shown in Figure S2 from the Supporting Information, the variations of H_C in that case are negligible, both for positive and negative applied voltages.

In order to rule out that oxidation/reduction reactions might govern the observed variations of H_C, cyclic electrochemical voltammetry experiments were performed, both for the nanoporous and the fully-dense Cu-Ni films, using the same non-aqueous electrolyte as for the magnetoelectric measurements. The results, shown in Figure S3 (see Supporting Information), indicate absence of clear oxidation/reduction peaks, with current densities of the order of $\mu A \cdot cm^{-2}$, varying smoothly with potential. This suggests that capacitive processes (i.e., charge accumulation), rather than faradaic ones (involving transfer of electrons across the metal-solution interface), dominate during in-situ magnetoelectric measurements. This is in agreement with XRD results since no diffraction peaks attributable to metal oxides were observed after the magnetoelectric measurements (see Figure 1e). No evidence for phase separation (i.e., occurrence of peaks from Ni-rich and Cu-rich FCC solid solutions) was encountered either after the magnetoelectric measurements. Additionally, the Cu/Ni ratio of the films did not vary after the measurements, confirming that no partial dissolution of the Cu-Ni porous film took place during the voltage application (i.e., the observed magnetic changes are not due to variations in the films compositions).

To further confirm that oxidation/reduction processes are not responsible for the observed trends in magnetic properties, hysteresis loops were also acquired while applying

voltage using an aqueous electrolyte (0.1 M NaOH solution). In this case, oxidation indeed takes place upon application of a positive potential, as evidenced by cyclic voltammetry (Figure S4a, Supporting Information), where relatively high current densities (~mA·cm^{-2}) are attained for $V > \pm 1$V. However, in spite of oxidation, the changes in H_C were always < 6% and actually H_C slightly increased (not decreased) after partial oxidation (Figure S4b, Supporting Information).

2.3. *Ab-initio* calculations

The fundamental physical origin of intrinsic magnetoelectric effects in metallic alloys remains still not fully understood. However, in metals, electric fields are screened very effectively and such screening is known to be spin-dependent due to exchange interactions.[16] Hence, the electrostatic charges that are accumulated at the surface (within the so-called Thomas-Fermi screening length, $\lambda_{TF} \sim 0.5$ nm) can induce modifications in the electronic band structure (i.e., in the charge density of unpaired *d* electrons with energy close to the Fermi level[13,16]) and, consequently, cause changes in the surface magnetization and the magnetic anisotropy energy (MAE).[16,30,31] Magnetic effects can propagate a few nm towards the interior of the alloy, within the spin-spin correlation length, which exceeds 20 nm in many metallic systems.[32] Given the 3D nanoporous morphology of the films, the electric field affects the nanopore walls from "all directions" (see Figure 2b). Interestingly, since the pore walls are very narrow and fully interconnected, the *overall* porous structure (i.e., the entire porous film) contributes to the observed voltage-induced large reduction of coercivity.

Although magnetoelectric phenomena in ultra-thin $Cu_{1-x}Ni_x$ films have been predicted theoretically (in particular, changes in the Curie temperature),[32] this is the first experimental demonstration of such effects for this type of alloys. To get a deeper understanding of the fundamental origin of magnetoelectric effects in Cu-Ni we carried out *ab-initio* calculations,[33,34] including spin-orbit interactions, on (111) slabs of $Cu_{25}Ni_{75}$ (**Figure 4a** and

4b). Different configurations of randomly arranged Cu and Ni atoms were averaged in order to simulate an alloy (three examples are depicted in Figure 4a). The results show an almost linear dependence of the surface magnetic moment with the applied electric field (Figure 4c), which can be quantified as:

$$\mu_0 \Delta M = \alpha_S E, \quad (1)$$

where ΔM is the surface magnetization, E the applied electric field and α_S is the so-called surface magnetoelectric coefficient. Note that E of the order of $1 V \cdot Å^{-1}$ indeed corresponds to the values obtained from voltages around 10 V (as in our experiments), assuming that the electrical double layer is approximately 1 nm thick.[29] Fitting the data in Figure 4c we obtain that $\alpha_S \approx 3.6 \times 10^{-14}$ $G \cdot cm^2 \cdot V^{-1}$ when the magnetic moment is in-plane, and $\alpha_S \approx 3.0 \times 10^{-14}$ $G \cdot cm^2 \cdot V^{-1}$ when the magnetic moment is pointing out-of-plane. These values are of the same order of magnitude as the ones calculated for a pure Fe(001) film.[30] Similar trends are obtained considering the (001) plane (see Figure S5). The applied electric field also induces changes in the density of states (Figure S6) and an increase of the change of the surface orbital moment m_L (Figure 4d), which can be related to an increase of the MAE using Bruno's relation:[35]

$$\text{MAE} \; \alpha \; \Delta m_L. \quad (2)$$

The changes in total and orbital magnetic moments shown in Figure 4 are confined to the surface atoms. Overall, the effect would be negligible, as shown in Figure S2 for a fully-dense film. The use of a nanoporous material allows enhancing the effect to make it measurable.

Changes in MAE are generally correlated with variations in H_C, M_R/M_S and χ (i.e., the overall shape and width of the loop).[13,16] However, in our case, due to the complex morphology of mesoporous Cu-Ni films, the correlation between MAE, H_C and χ is not straightforward. An increase of positive MAE indicates an enhancement of perpendicular magnetocrystalline anisotropy per Ni atom. Magnetocrystalline anisotropy competes with the

shape anisotropy (which promotes magnetic easy axis along the nanopores ligaments directions, which are randomly distributed). Such competing anisotropies make the correlation between H_C and MAE rather complex. Nonetheless, the variation of H_C and χ with the electric field can be considered consistent with changes in the calculated MAE of the system.

3. Conclusions

In conclusion, our work demonstrates that the coercivity of nanoporous Cu-Ni thick films can be drastically decreased by simply applying an electric field. The large surface-area-to-volume ratio and the ultra-narrow pore walls of the system play a crucial role in the discovered effect. Such electrically-driven modification of magnetic properties is very appealing for energy-efficient magnetic actuation. Indeed, a reduction in coercivity implies that lower currents are needed to switch the magnetization of the system (either when using an electromagnet or in spin-torque devices), hence considerably reducing energy loss in the form of heat dissipation (Joule effect). The voltage-induced decrease of coercivity could also be used as an alternative to thermally-assisted magnetic writing in magnetic recording applications, since the latter is less energetically effective. Thus, the results from this work will likely expand the already wide range of applications of nanoporous materials (so far, mainly in chemistry), to areas like magnetically-actuated micro-electro-mechanical systems, magnetic recording or spintronics, where their potential has been hitherto largely overlooked.

4. Experimental Section

4.1. Nanoporous Cu-Ni Film growth

The electrodeposition of nanoporous Cu-Ni films was performed in a thermostatized three-electrode cell using a PGSTAT302N Autolab potentiostat/galvanostat (Ecochemie). Contrary to other more sophisticated methods, here the nanoporosity is induced during single-step micelle-assisted electrodeposition (see Figure 1a), a procedure which has been used in recent

years for the growth of only very few types of nanoporous layers, i.e., Pt-based alloys[36-38] and Cu[39], but not magnetic alloys. Together with the lyotropic liquid crystals (LLC), this synthetic approach can be categorized as a soft templating method. Above the "critical micellar concentration" (c.m.c.) (e.g., 0.004 wt.% for P123 at room temperature[40]), the micelles start to spontaneously form in the aqueous solution, get progressively in contact and tend to self-assemble at the solid-liquid interface, interfering and guiding the electrodeposition process, leading to the growth of mesoporous metallic films (see Figure 1a). Si/SiO_2 chips coated with Ti (10 nm)/Au (90 nm) adhesion/seed layers were used as cathodes (0.25 cm^2 working area), a platinum spiral served as counter electrode and a double junction Ag|AgCl (E = +0.210 V/SHE) with 3 M KCl inner solution and 1 M $NaSO_4$ outer solution was employed as the reference electrode (Metrohm AG). Prior to deposition, the substrates were degreased with acetone and ethanol, and rinsed in Milli-Q water. The electrolyte contained 0.2 M $Ni(CH_3COO)_2 \cdot 4H_2O$, 0.02M $CuSO_4 \cdot 5H_2O$ and 8 $mg \cdot mL^{-1}$ (0.8 wt%) of poly(ethylene oxide)-block-poly(propylene oxide)-block-poly(ethylene oxide) (PEO-PPO-PEO) tri-block co-polymer (Pluronic®P-123). The pH was left as-prepared (pH = 6.0). Electrodeposition was carried out galvanostatically at a current density (j) of -80 $mA \cdot cm^{-2}$ during 120 s under mild agitation (200 rpm) to favour mass transport of the electroactive species toward the cathode. N_2 was bubbled through the solution to get rid of oxygen before each deposition. The electrodeposited films were rinsed with milli-Q water and ultrasonicated in ethanol for 5 min to remove remaining micelles from the growth process.

4.2. Fully-dense Cu-Ni Film growth

The electrodeposition of fully-dense Cu-Ni films is described elsewhere.[27]

4.3. Magnetoelectric measurements

Hysteresis loops at different DC voltage values were measured at room temperature, along the film plane, in a Magneto-Optic Kerr Effect (MOKE) setup from Durham Magneto-Optics (see

Figure 2a). An external Agilent B2902A power supply was employed to generate voltage. The sample was mounted vertically in a quartz SUPRASIL® cell filled with anhydrous propylene carbonate containing Na^+ ions. The anhydricity of the electrolyte avoided oxidation of the Cu-Ni during magnetoelectric measurements. Metallic sodium ions played a two-fold role: (i) to react with any trace amounts of water that could enter the electrochemical system during experimental manipulation, forming Na^+OH^-; (ii) to promote the creation of the electrical double layer from the solvated Na^+ and OH^- ions. A waiting time of 300 s was introduced between each voltage change and the hysteresis loop measurement in order to allow the diffusion of the electrolyte towards the interior of the pores of the Cu-Ni film and the formation of the electrical double layer. For the sake of comparison, magnetoelectric experiments were also carried out using a 0.1M NaOH solution that forced sample oxidation during voltage application. The oxidation potentials were selected in agreement with cyclic voltammetry results.

4.4. Morphology and structural characterization

The morphology of the nanoporous films was assessed by high resolution transmission electron microscopy (HRTEM, FEI Tecnai G2 F20 operated at 200 kV) and scanning transmission electron microscopy (STEM, model FEI Tecnai F20) and compositional analyses were performed using energy-dispersive X-ray analysis (EDX) in a field emission scanning electron microscope (Zeiss Merlin, at 2kV and 100pA). The crystal structure was investigated by X-ray diffraction (XRD) on a Philips X'Pert diffractometer (Panalytical) using Cu-K_α radiation, in the 42-54° 2θ range.

4.5. Electrochemical characterization

Cyclic voltammetries were carried out in a PGSTAT 302 N Autolab potentiostat/galvanostat (Ecochemie) and a VSP potentiostat with low-current option from BIOLOGIC.

4.6. Ab-initio calculations

First principles calculations were performed by means of density functional theory (DFT) using the SIESTA code.[33,34] Norm–conserving Troulliers-Martins pseudopotentials[41] including pseudocore corrections were used to describe the core electrons, and double–zeta polarized strictly localized numerical atomic orbitals were used as basis set. An additional shell of diffuse orbitals was used in the surface atoms, as described in Ref. 42, to improve the accuracy of the description of the surface properties. The generalized gradient approximation in the Perdew–Burke-Ernzerhof (PBE) version was used for the exchange correlation potential.[43] Spin-orbit interactions were included in the on–site approximation.[44,45] An electric field was applied perpendicular to the film. Exhaustive convergence tests were performed to guarantee a tolerance below 10^{-5} eV in the total energies and below 10^{-3} μ_B in the spin and orbital moments. To achieve that level of convergence a 25x25x1 k-grid was used, together with a temperature of 1 K in the Fermi–Dirac distribution and a mesh grid of 600 Ry.

A FCC $Cu_{25}Ni_{75}$ alloy was simulated using a (2x2) 10 layer slab with randomly arranged Cu and Ni atoms. The lattice constant of 3.542 Å was obtained from experimental data at this concentration.[27] Symmetry was applied, so up and down surfaces were equivalent. In this way results for positive and negative electric fields were extracted from a single calculation. Several atomic configurations were considered for the (111) orientation and the results were averaged among them. A single configuration was considered for the (001) orientation to show that the results are qualitatively similar for both orientations (see Figure S5 in the Supporting Information).

The magnetic density of states (MDOS) (Figure S6) was calculated as the density of states for spin up minus the density of states for spin down projected in the direction of the magnetization.

Supporting Information

Supporting Information is available from the Wiley Online Library or from the author.

Acknowledgements

Financial support by the European Research Council (SPIN-PORICS 2014-Consolidator Grant, Agreement nº 648454), the Spanish Government (Projects MAT2014-57960-C3-1-R and FIS2015-64886-C5-3-P and associated FEDER) and the Generalitat de Catalunya (2014-SGR-1015 and 2014-SGR-301) is acknowledged. E. M. acknowledges the European Union's Horizon 2020 research and innovation programme under the Marie Skłodowska-Curie grant agreement Nº 665919. E.P. is grateful to MINECO for the "Ramon y Cajal" contract (RYC-2012-10839). E.I.C. acknowledges the grant awarded by the National Council on Science and Technology in Mexico (CONACYT). The authors would also like to acknowledge networking support by the COST Action e-MINDS MP1407. ICN2 acknowledges the support from the Severo Ochoa Program (MINECO, grant SEV-2013-0295). A. Quintana and Dr. J. Zhang equally contributed to this work.

Received: ((will be filled in by the editorial staff))
Revised: ((will be filled in by the editorial staff))
Published online: ((will be filled in by the editorial staff))

References

[1] I. Zútic, J. Fabian, S. Das Sarma, *Rev. Mod. Phys.* **2004**, *76*, 323.

[2] C. Chappert, A. Fert, F. N. Van Dau, *Nat. Mater*. **2007**, *6*, 813.

[3] J.-M. Hu, Z. Li, L.-Q. Chen, C.-W. Nan, *Nat. Commun.* **2011**, *2*, 553.

[4] S. Urazhdin, V. E. Demidov, H. Ulrichs, T. Kendziorczyk, T. Kuhn, J. Leuthold, G. Wilde, S. O. Demokritov, *Nat. Nanotechnol*. **2014**, *9*, 509.

[5] B. Dieny, R. C. Sousa, J. Hérault, C. Papusoi, G. Prenat, U. Ebels, D. Houssameddine, B. Rodmacq, S. Auffret, L. D. Buda-Prejbeanu, *Int. J. Nanotechnol*. **2010**, *7*, 591.

[6] Y. Wang, J. Hu, Y. Lin, C.-W. Nan, *NPG Asia Mater*. **2010**, *2*, 61.

[7] H. K. D. Kim, L. T. Schelhas, S. Keller, J. L. Hockel, S. H. Tolbert, G. P. Carman, *Nano Lett*. **2013**, *13*, 884.

[8] R. Ramesh, N. A. Spaldin, *Nat. Mater.* **2007**, *6*, 21.

[9] U. Bauer, L. Yao, A. J. Tan, P. Agrawal, S. Emori, H. L. Tuller, S. van Dijken, G. S. D. Beach, *Nat. Mater.* **2015**, *14*, 174.

[10] D. A. Gilbert, A. J. Grutter, E. Arenholz, K. Liu, B. J. Kirby, J. A. Borchers , B. B. Maranville, *Nat. Commun.* **2016**, *7*, 12264.

[11] H. Ohno, D. Chiba, F. Matsukura, T. Omiya, E. Abe, T. Dietl, Y. Ohno, K. Ohtani, *Nature* **2000**, *408*, 944.

[12] D. Chiba, M. Sawicki, Y. Nishitani, Y. Nakatani, F. Matsukura, H. Ohno, *Nature* **2008**, *455*, 515.

[13] M. Weisheit, S. Fähler, A. Marty, Y. Souche, C. Poinsignon, D. Givord, *Science* **2007**, *315*, 349.

[14] T. Maruyama, Y. Shiota, T. Nozaki, K. Ohta, N. Toda, M. Mizuguchi, A. A. Tulapurkar, T. Shinjo, M. Shiraishi, S. Mizukami, Y. Ando, Y. Suzuki, *Nat. Nanotechnol.* **2009**, *4*, 158.

[15] D. Chiba, S. Fukami, K. Shimamura, N. Ishiwata, K. Kobayashi, T. Ono, *Nat. Mater.* **2011**, *10*, 853.

[16] O. O. Brovko, P. Ruiz-Díaz, T. R. Dasa, V. S. Stepanyuk, *J. Phys.: Condens. Matter* **2014**, *26*, 093001.

[17] W.-G. Wang, M. Li, S. Hageman, C. L. Chien, *Nat. Mater*. **2012**, *11*, 64.

[18] F. Bonell, S. Murakami, Y. Shiota, T. Nozaki, T. Shinjo, Y. Suzuki, *Appl. Phys. Lett*. **2011**, *98*, 232510.

[19] F. Matsukura, Y. Tokura, H. Ohno, *Nat. Nanotechnol*. **2015**, *10*, 209.

[20] B. Jiang, C. Li, V. Malgras, M. Imura, S. Tominaka, Y. Yamauchi, *Chem. Sci.* **2016**, *7*, 1575.

[21] L. Wang, Y. Yamauchi, *J. Am. Chem. Soc*. **2013**, *135*, 16792.

[22] D. Gu, F. Schüth, *Chem. Soc. Rev*. **2014**, *43*, 313.

[23] T. Wagner, S. Haffer, C. Weinberger, D. Klaus, M. Tiemann, *Chem. Soc. Rev.* **2013**, *42*, 4036.

[24] J. Zhang, C. M. Li, *Chem. Soc. Rev*. **2012**, *41*, 7016.

[25] T. E. Quickel, L. T. Schelhas, R. A. Farrell, N. Petkov, V. H. Le, S. H. Tolbert, *Nat. Commun*. **2015**, *6*, 6562.

[26] S. Gosh, *J. Magn. Magn. Mater*. **2011**, *323*, 552.

[27] E. Pellicer, A. Varea, S. Pané, B. J. Nelson, E. Menéndez, M. Estrader, S. Suriñach, M. D. Baró, J. Nogués, J. Sort, *Adv. Funct. Mater*. **2010**, *20*, 983.

[28] E. Pellicer, A. Varea, K. M. Sivaraman, S. Pané, S. Suriñach, M. D. Baró, J. Nogués, B. J. Nelson, J. Sort, *ACS Appl. Mater. Interfaces* **2011**, *3*, 2265.

[29] K. Bohinc, V. Kralj-lglic, A. Iglic, *Electrochim. Acta* **2001**, *46*, 3033.

[30] K. Nakamura, R. Shimabukuro, Y. Fujiwara, T. Akiyama, T. Ito, *Phys. Rev. Lett.* **2009**, *102*, 187201.

[31] C.-G. Duan, J. P. Velev, R. F. Sabirianov, Z. Zhu, J. Chu, S. S. Jaswal, E. Y. Tsymbal, *Phys. Rev. Lett.* **2008**, *101*, 137201.

[32] I. V. Ovchinnikov, K. L. Wang, *Phys. Rev. B* **2009**, *79*, 020402.

[33] J. M. Soler, E. Artacho, J. D. Gale, A. García, J. Junquera, P. Ordejón, D. Sánchez-Portal, *J. Phys.: Condens. Matter* **2002**, *14***,** 2745.

[34] E. Artacho, E. Anglada, O. Diéguez, J. D. Gale, A. García, J. Junquera, R. M. Martin, P. Ordejón, J. M. Pruneda, D. Sánchez-Portal, J. M. Soler, *J. Phys.: Condens. Matter* **2008**, *20*, 064208.

[35] P. Bruno, *Phys. Rev. B* **1989**, *39*, 865.

[36] H. Wang, L. Wang, T. Sato, Y. Sakamoto, S. Tominaka, K. Miyasaka, N. Miyamoto, Y. Nemoto, O. Terasaki, Y. Yamauchi, *Chem. Mater.* **2012**, *24*, 1591.

[37] H. Wang, S. Ishihara, K. Ariga, Y. Yamauchi, *J. Am. Chem. Soc.* **2012**, *134*, 10819.

[38] V. Malgras, H. Ataee-Esfahani, H. Wang, B. Jiang, C. Li, K. C.-W. Wu, J. H. Kim, Y. Yamauchi, *Adv. Mater.* **2016**, *28*, 993.

[39] C. Li, B. Jiang, Z. Wang, Y. Li, Md. S. A. Hossain, J. H. Kim, T. Takei, J. Henzie, O. Dag, Y. Bando, Y. Yamauchi, *Angew. Chem. Int. Ed.* **2016**, *55*, 12746.

[40] G. Wanka, H. Hoffmann, W. Ulbricht, *Macromolecules* **1994**, *27*, 4145.

[41] N. Troullier, J. L. Martins, *Phys. Rev. B* **1991**, *43*, 1993.

[42] S. García-Gil, A. García, N. Lorente, P. Ordejón, *Phys. Rev. B* **2009**, *79*, 075441.

[43] J. P. Perdew, K. Burke, M. Ernzerhof, *Phys. Rev. Lett.* **1996**, *77*, 3865.

[44] L. Fernández-Seivane, M. A. Oliveira, S. Sanvito, J. Ferrer, *J. Phys.: Condens. Matter*

2006, *18*, 7999.

[45] L. Fernández-Seivane, J. Ferrer, *Phys. Rev. Lett.* **2007**, *99*, 183401.

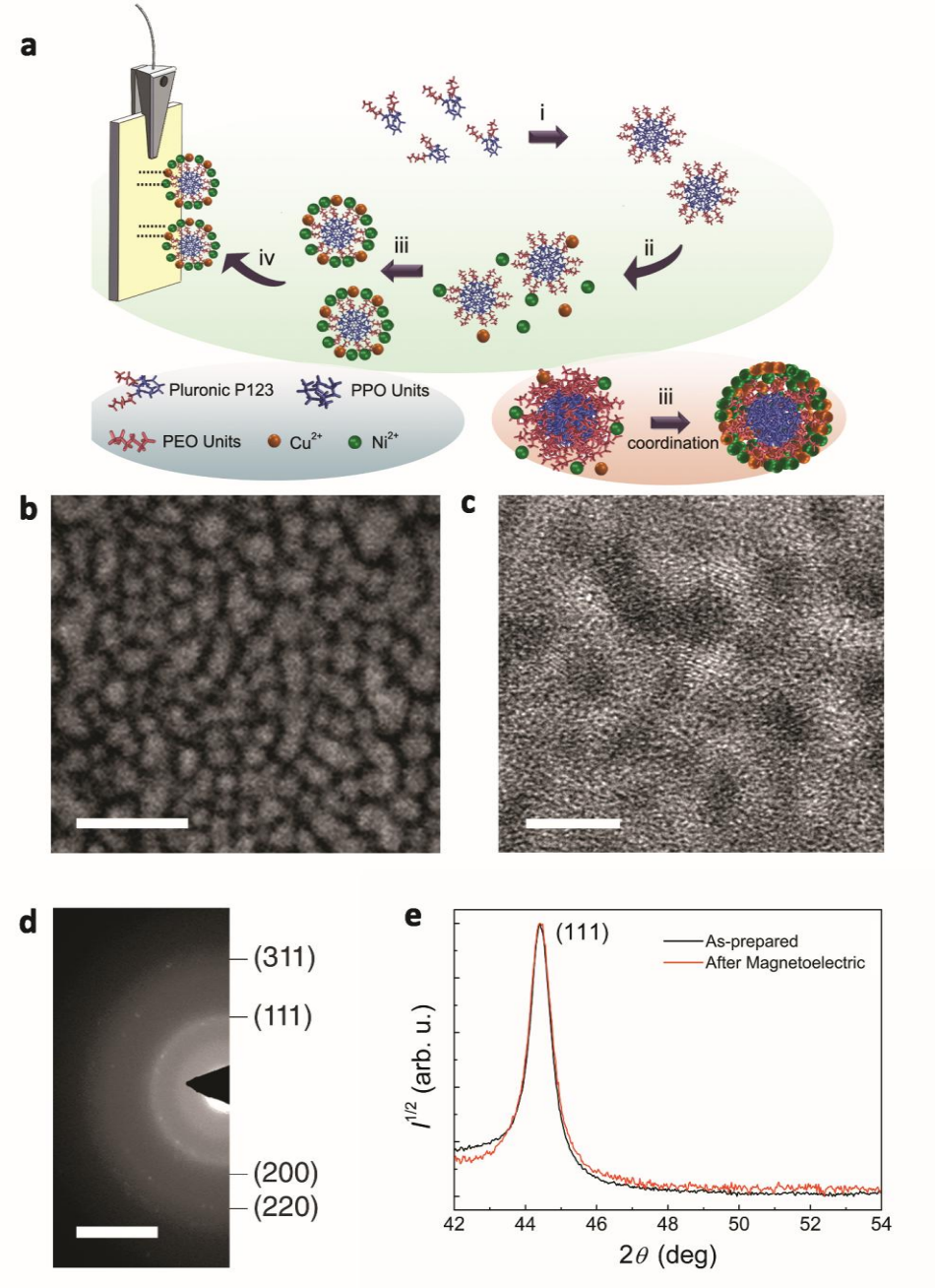

Figure 1. (a) Illustration of the micelle-assisted electrodeposition procedure, where PPO and PEO denote, respectively, the poly(ethylene oxide) and poly(propylene oxide) blocks of the Pluronic®P-123 tri-block co-polymer and (i-iv) denote the different synthetic steps: i) stirring for clear solution, ii) addition of metal salt, iii) coordination of dissolved metal species with the hydrophilic shell domains of the micelles, iv) electrodeposition. (b) Cross-section image of the electrodeposited nanoporous Cu-Ni films, observed by scanning transmission electron microscopy (STEM) –image taken from the middle depth of the films. (c) High-resolution transmission electron microscopy (HRTEM) image of the nanoporous Cu-Ni alloy. (d) Corresponding selected area diffraction (SAED) pattern. (e) X-ray diffraction (XRD) patterns of the nanoporous films before and after the magnetoelectric measurements. Note that the scale bars in (b), (c) and (d) are 25 nm, 5 nm and 5 nm^{-1}, respectively.

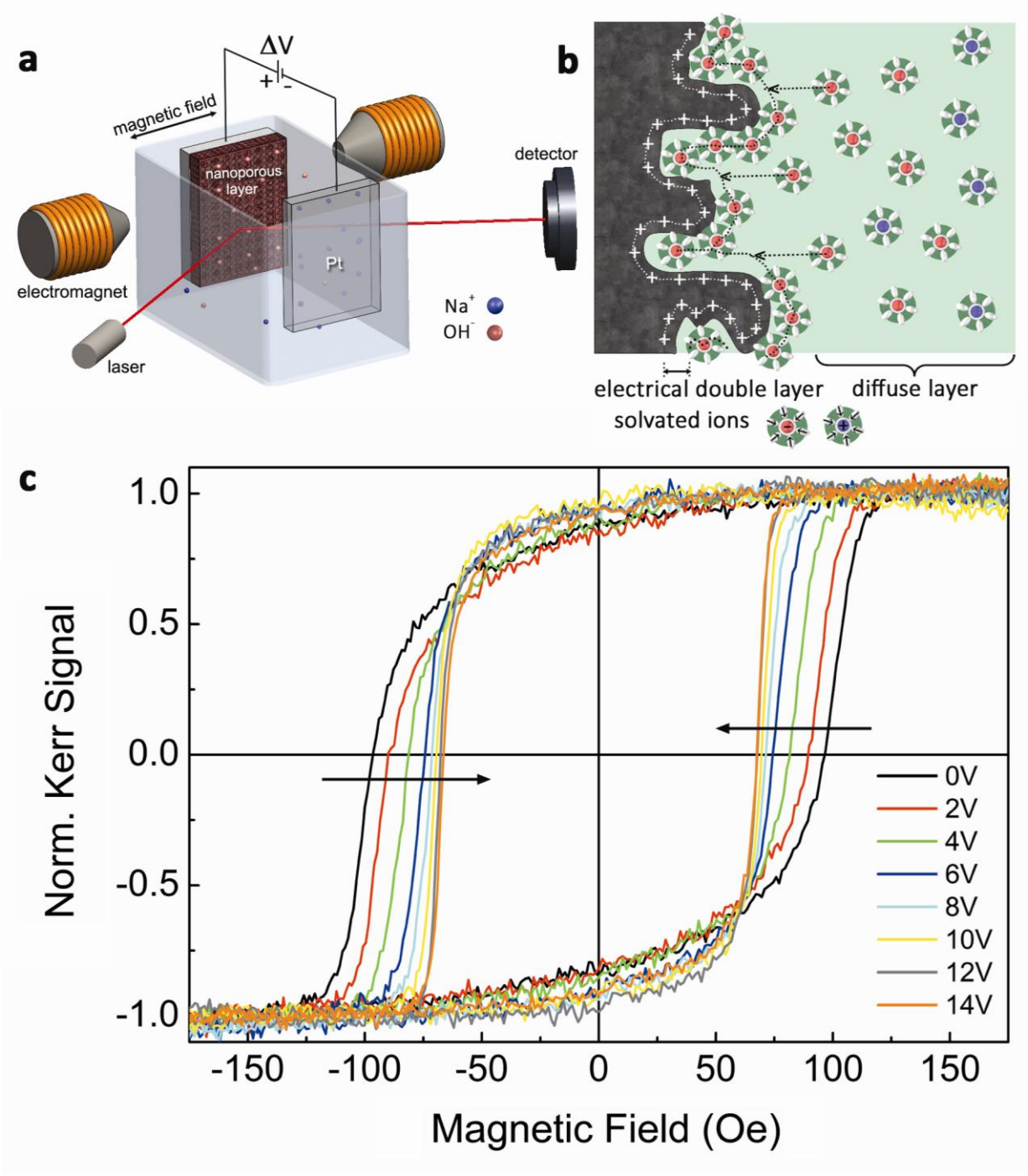

Figure 2. (a) Schematic illustration of the experimental setup used for the magnetoelectric measurements. (b) Representation of the formation of the electrical double layer around the pore walls during the magnetoelectric measurements. (c) Representative hysteresis loops of the nanoporous Cu-Ni films acquired under application of different voltage values.

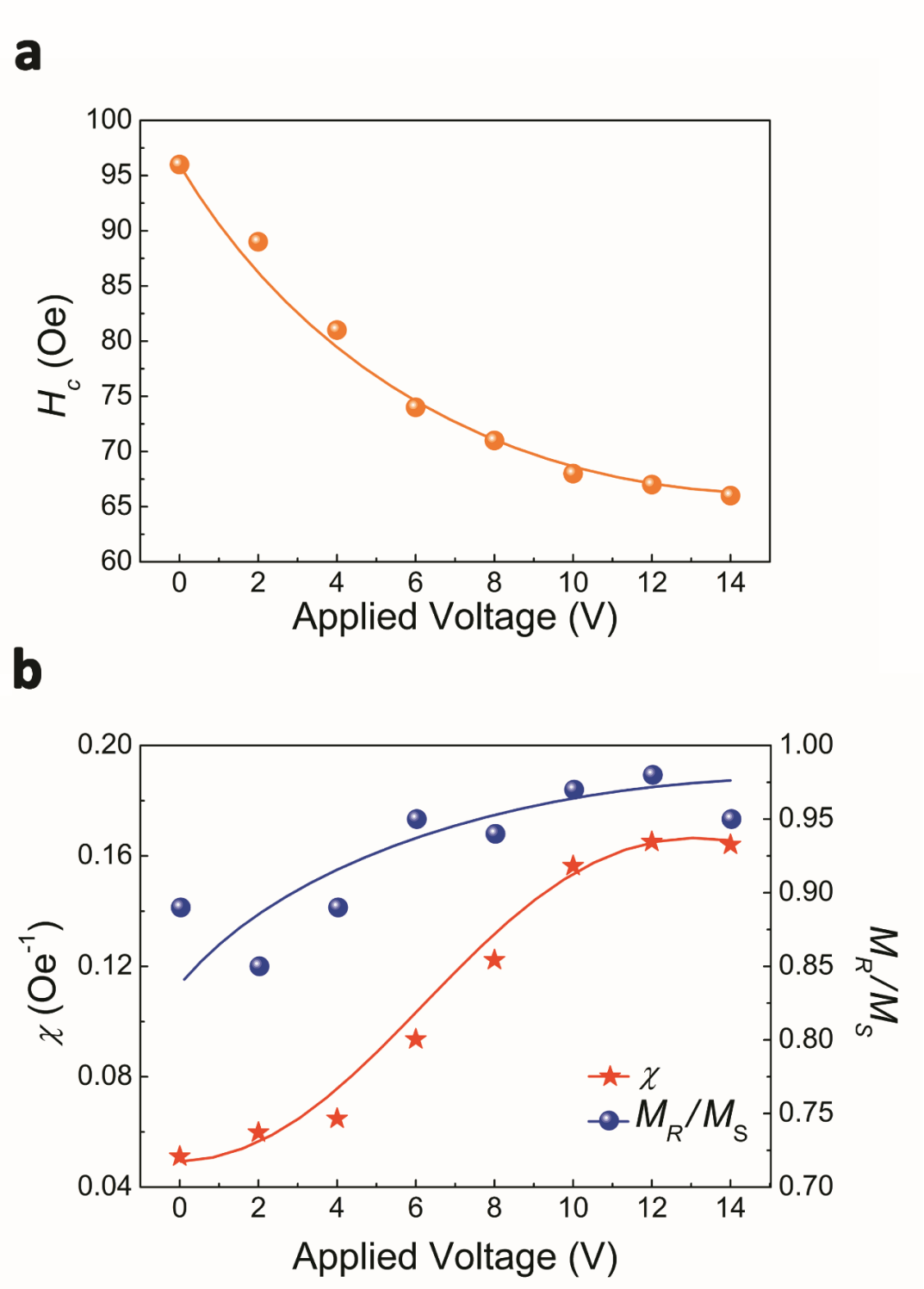

Figure 3. (a) Dependence of the coercivity, H_C, on the applied positive voltage. (b) Dependence of the susceptibility around the coercivity (see definition in the text), χ , and the remanence-to-saturation magnetization ratio, M_R/M_S, as a function of voltage. Note that the lines are guides to the eye.

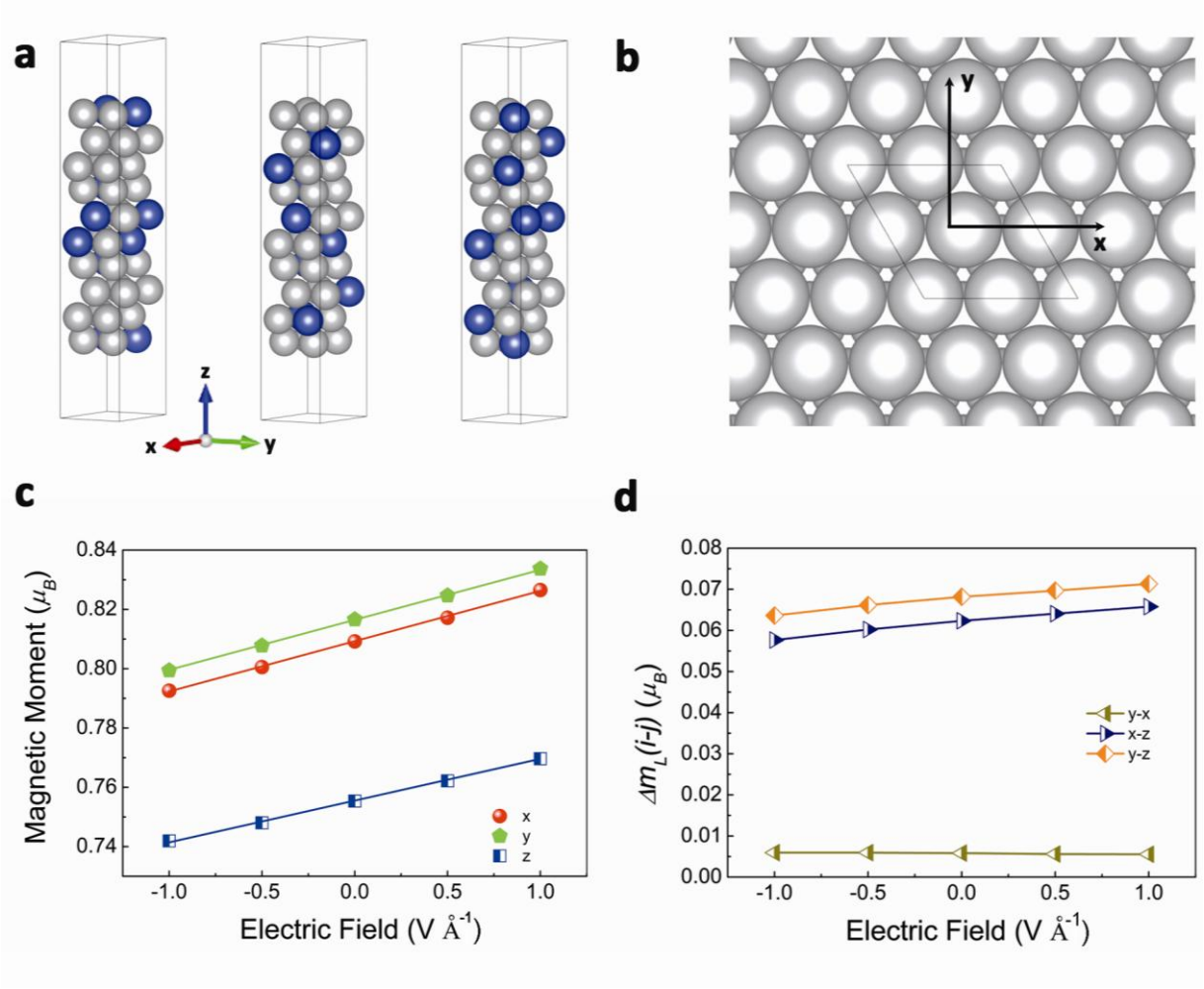

Figure 4. (a) Representative configurations, corresponding to the (111) orientation with different positions for Cu and Ni atoms within the lattice, which were considered for the *ab-initio* calculations. Blue (grey) spheres represent Cu (Ni) atoms. (b) In-plane directions considered for the (111) surface. The *z* direction is perpendicular to the plane. (c) Dependence with the applied electric field of the magnetic moment oriented along the given directions for the Ni surface atoms. The lines are guides to the eye. (d) Orbital moment differences Δm_L between the indicated directions for the surface Ni atoms. The lines are guides to the eye. According to Bruno's relation higher orbital moments correspond to lower energies in the corresponding magnetization direction.

Table of contents entry:

A novel effect in nanoporous magnetic films is demonstrated: the possibility to drastically reduce their coercivity under the action of an electric field, by simply applying continuous voltage. The reduction of coercivity with voltage implies that lower currents are needed to switch the magnetization of the system, thus considerably reducing heat dissipation and enhancing energy efficiency during magnetic actuation.

Keywords: nanoporous alloys, magnetic actuation, magneto-electric effect, coercivity, energy efficiency

Alberto Quintana, Jin Zhang, Eloy Isarain-Chávez, Enric Menéndez, Ramon Cuadrado, Roberto Robles*, Maria Dolors Baró, Miguel Guerrero, Salvador Pané, Bradley J. Nelson, Carlos M. Müller, Pablo Ordejón, Josep Nogués*, Eva Pellicer*, Jordi Sort*

Voltage-induced coercivity reduction in nanoporous alloy films: a boost towards energy-efficient magnetic actuation

ToC figure

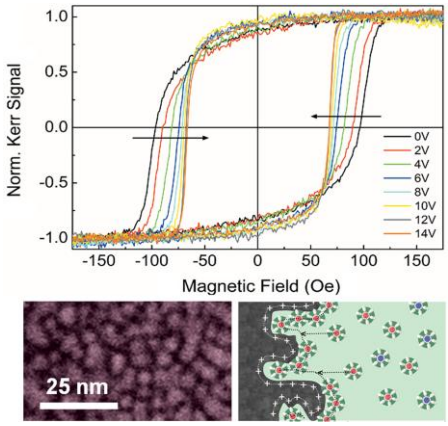

Supporting Information

Voltage-induced coercivity reduction in nanoporous alloy films: a boost towards energy-efficient magnetic actuation

Alberto Quintana, Jin Zhang, Eloy Isarain-Chávez, Enric Menéndez, Ramon Cuadrado, Roberto Robles, Maria Dolors Baró, Miguel Guerrero, Salvador Pané, Bradley J. Nelson, Carlos M. Müller, Pablo Ordejón, Josep Nogués*, Eva Pellicer*, Jordi Sort**

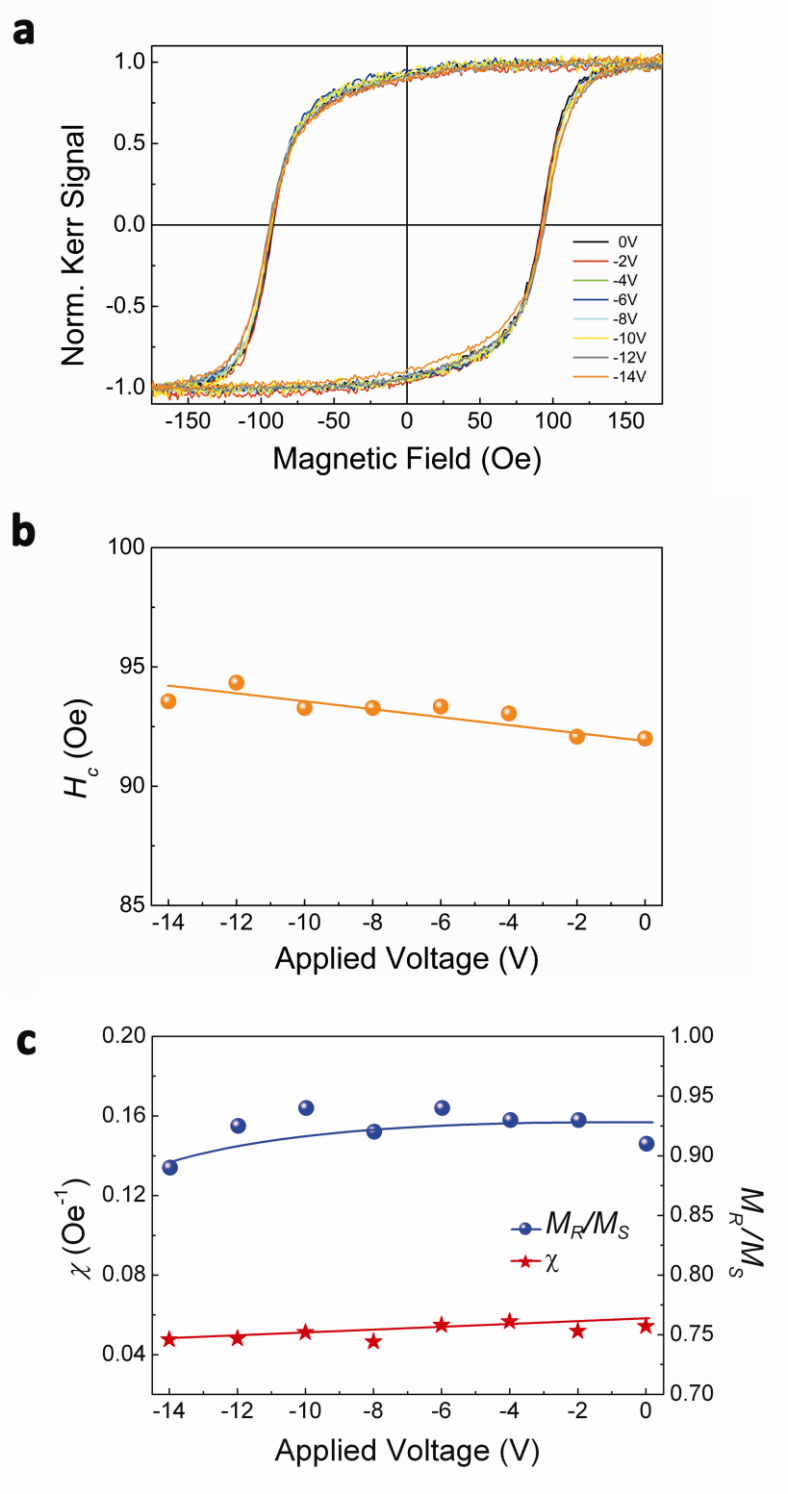

Figure S1. (a) Representative hysteresis loops of the nanoporous Cu-Ni films acquired under application of different negative voltage values. (b) Dependence of the coercivity, H_C, on the negative applied voltage. (c) Dependence of the susceptibility around coercivity (see definition in the text), χ , and the remanence-to-saturation magnetization ratio, M_R/M_S, as a function of negative voltage. Note that the lines in (b) and (c) are guides to the eye.

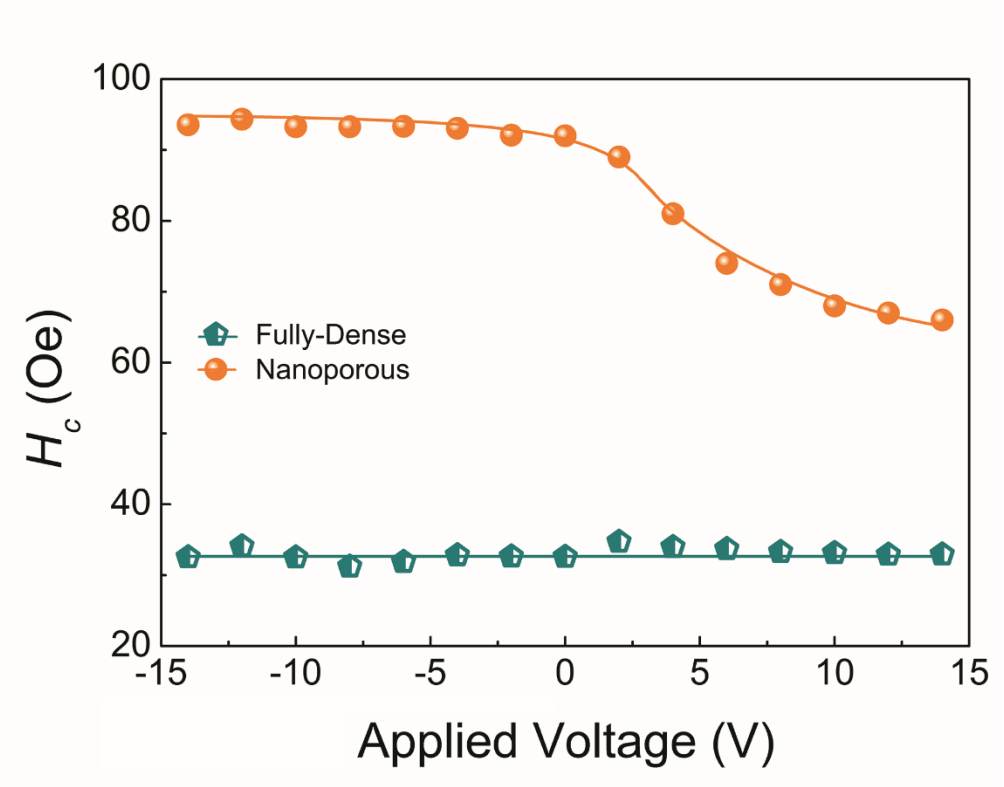

Figure S2. Dependence of the coervivity, H_C, on the applied voltage (both for negative and positive values), for the fully-dense and nanoporous Cu-Ni electrodeposited films with the same composition ($Ni_{75}Cu_{25}$ at.%) and thickness (600 nm).

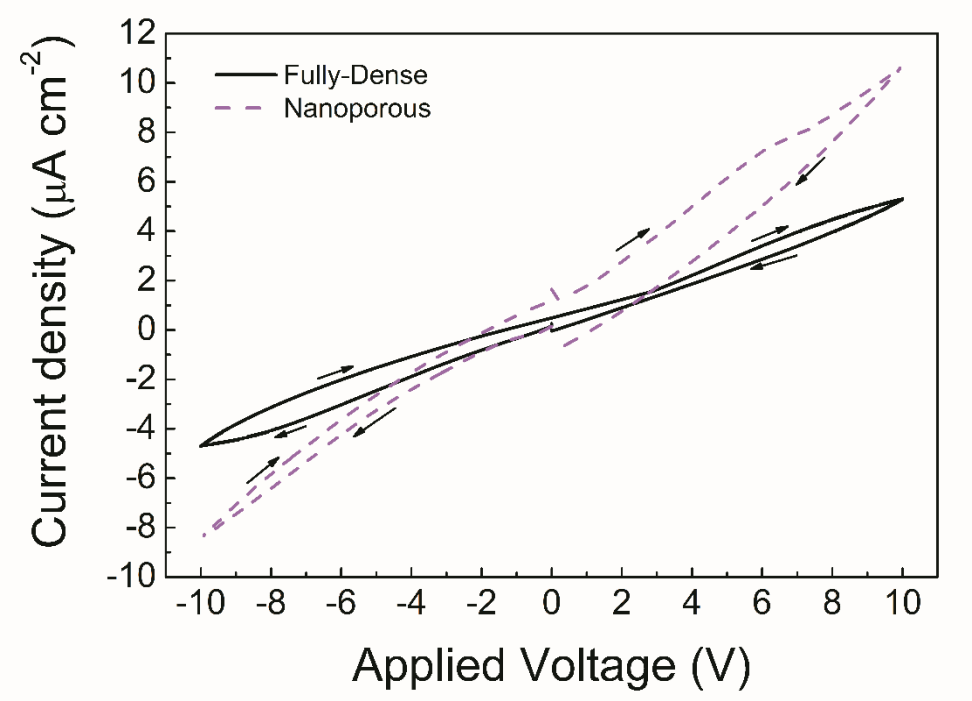

Figure S3. Cyclic voltammetry curves, measured while immersing the Cu-Ni films in the anhydrous electrolyte (propylene carbonate), for both nanoporous and fully-dense films.

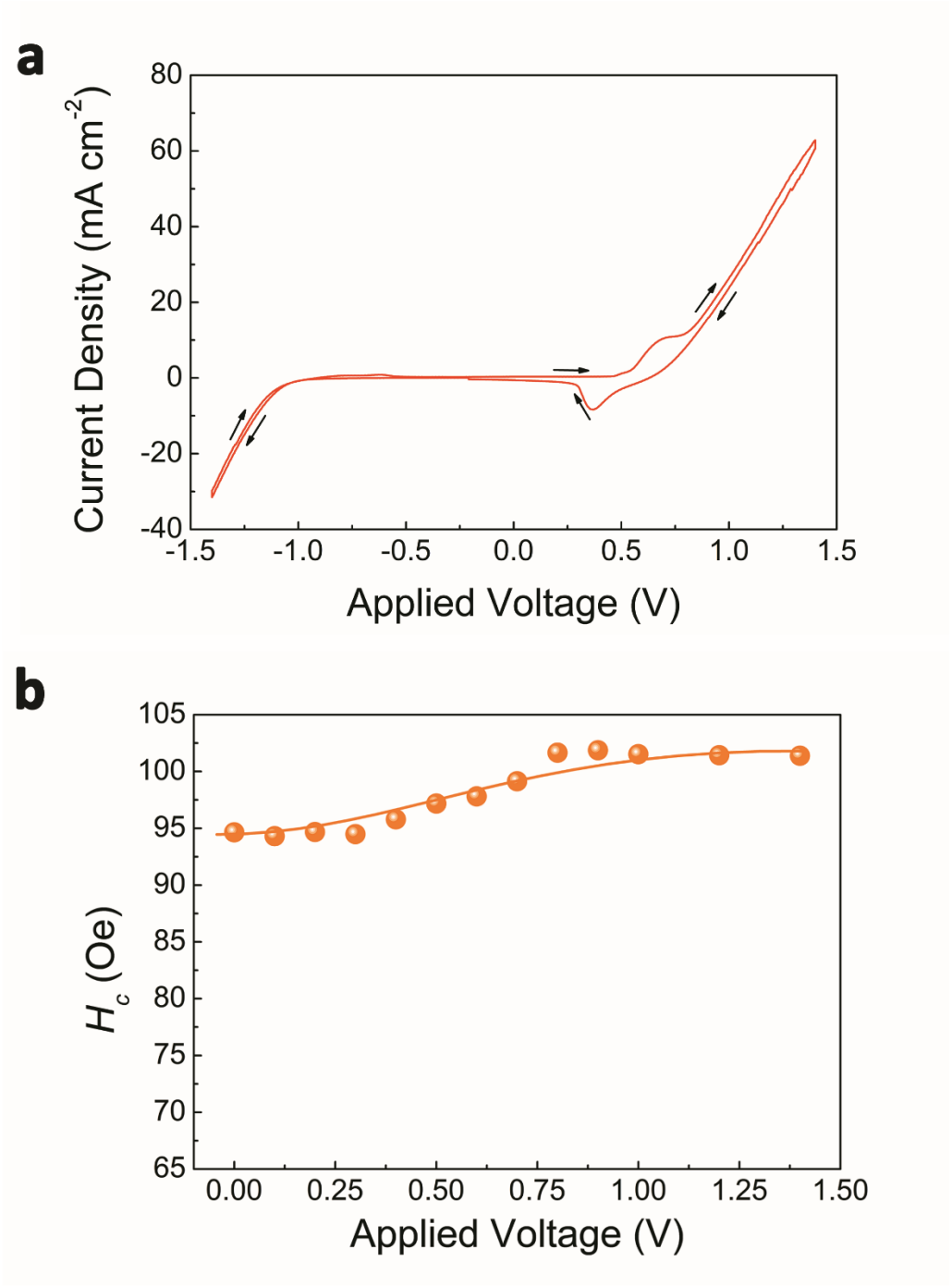

Figure S4. (a) Cyclic voltammetry curves from the nanoporous Cu-Ni films acquired while immersing the films in the aqueous electrolyte (0.1M NaOH). (b) Dependence of the coercivity, H_C, on the applied voltage when using the aqueous electrolyte. The line in (b) is a guide to the eye.

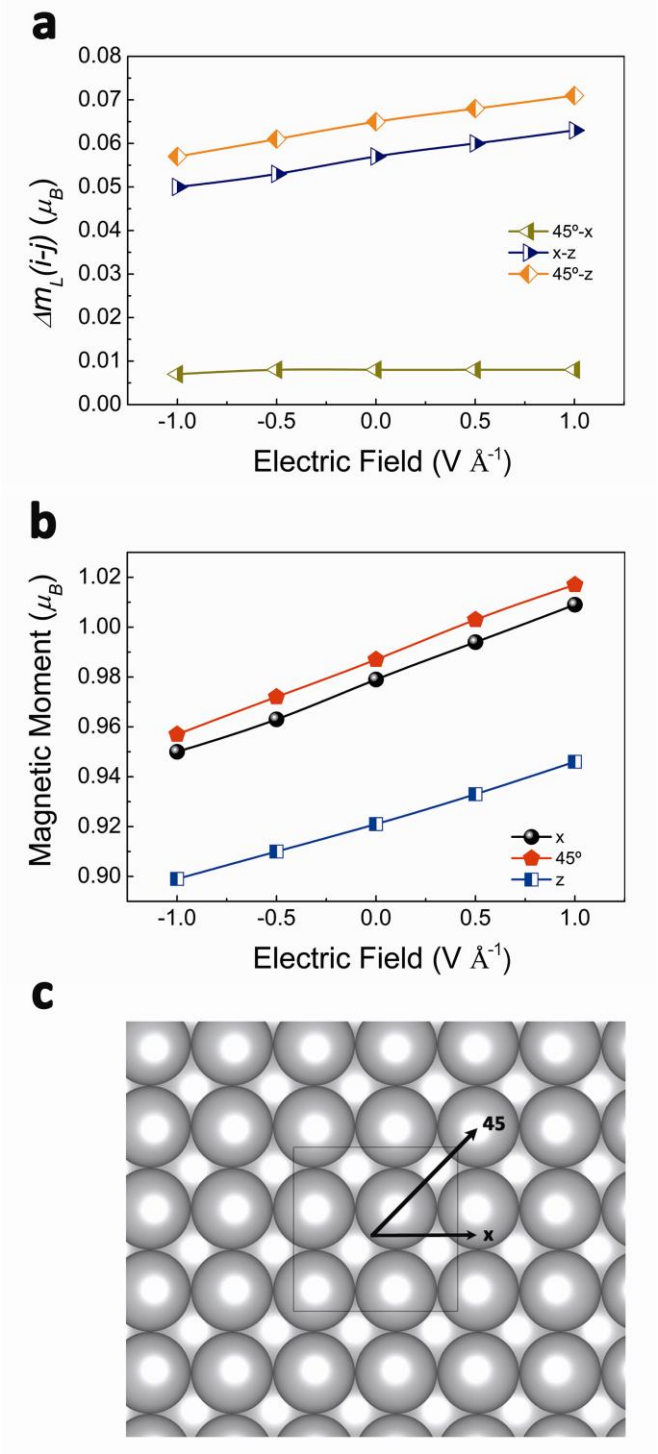

Figure S5. (a) Dependence of the magnetic moment oriented along the given directions of the (001) surface with the applied electric field. Only the surface Ni atoms are considered. The calculated surface magnetoelectric coefficients are $\alpha_S \approx 5.5\times10^{-14}$ G cm$^2\cdot$V^{-1} in-plane and $\alpha_S \approx 4.3\times10^{-14}$ G cm$^2\cdot$V^{-1} out-of-plane. (b) Orbital moment differences Δm_L between the indicated directions of the (001) surface for the surface Ni atoms. (c) In-plane directions considered for the (001) surface. The lines in (a) and (b) are guides to the eye.

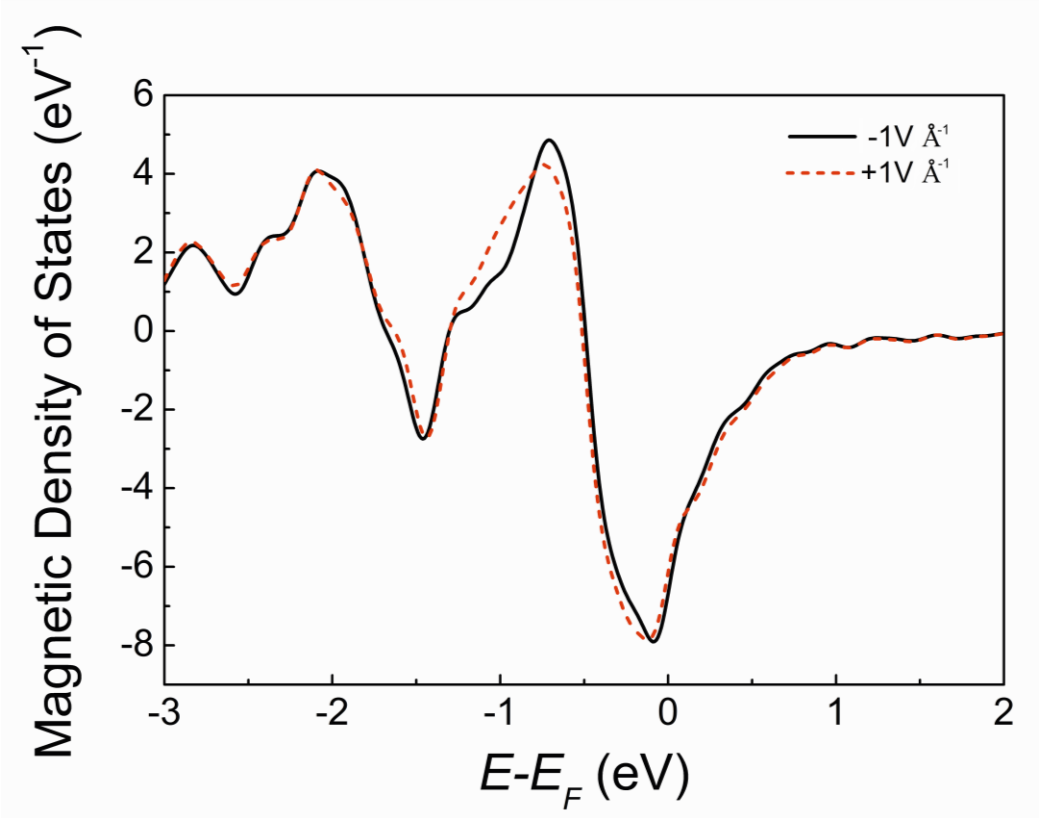

Figure S6. Magnetic density of states (MDOS) for the surface Ni atoms of one considered (111) configuration. MDOS is defined as the DOS for spin up minus DOS for spin down. Changes of the MDOS with the applied electric field illustrate the origin of the magnetoelectric effect.